National Aeronautics and Space Administration

Orbital Debris Quarterly News

Volume 22, Issue 3
September 2018

Inside...

A SOZ Unit Breakup Predicted and Observed in May 2018 2
Space Debris Sensor On-orbit Status 2
Spacecraft Material Ablation Testing at UT Austin 3
NASA ODPO's Large Constellation Study 4
ORDEM Interpolation—a Review and Prospectus 8
Orbital Debris Analyst 9
Conference and Workshop Reports 10
Space Missions and Satellite Box Score 12

A publication of the NASA Orbital Debris Program Office

CZ-4C Upper Stage Fragments in August

A Long March-4C (LM-4C or CZ-4C) third stage fragmented at 08:46Z on 17 August 2018 after approximately 4.74 years on orbit. This -4C model's event follows on single known fragmentations each of the CZ-4A (International Designator 1990-081D) and CZ-4B (1999-057C) third stages.

This stage (2013-065B, U.S. Strategic Command [USSTRATCOM] Space Surveillance Network [SSN] catalog number 39411) launched the Yaogan 19 Earth observing spacecraft.

At the time of the event, the stage was in a 1205.5- x 996.7-km altitude orbit at an inclination of 100.5°. At the current time six fragments are tracked. The ODQN will advise the readership of fragment tally as this event is better characterized.

The stage has an overall length of approximately 5 m, a diameter of 2.9 m, and a dry mass of approximately 1700 kg [1]. There may be 200-300 kg of residual propellants following payload separation; the fuel and oxidizer tanks share a common bulkhead, a design feature in common with the Delta II, Ariane 1-4, and other upper stages. The stage is also equipped with a monopropellant attitude control engine subsystem (ACES) and small solid rockets. Nominal post-separation passivation operations include ACES orientation of the vehicle to prevent plume impingement on the payload; leaving the operational orbit by firing the solid rockets; venting the main engines; and venting the ACES and He pressurant. This stage likely engaged in post-separation activities as its perigee was approximately 200 km lower than the payload. At the present time, however, an explosion attributable to on-board stored energy is the likely cause.

Reference

1. Yanfeng, G., W. Yijin, and F. Hongtuan, "Passivation Investigation and Engineering Applications for Orbital Stage of LM-4B/-4C Launch Vehicle," Space Debris Research, Special 2013, Chinese National Space Agency (2013), pp. 3-6. ♦

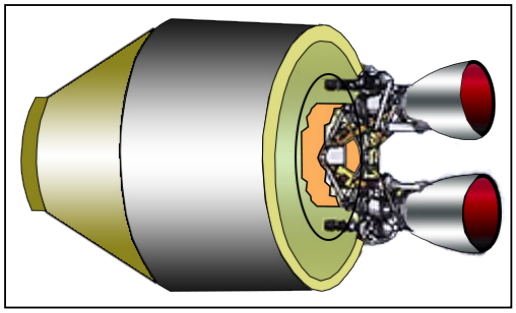

The Long March-4B/-4C upper stage; the -4C is equipped with two restart-capable YF-40A hypergolic liquid engines, a DT-3 monopropellant/He pressurized attitude control engine subsystem (ACES), and small solid rockets for separation.

A SOZ Unit Breakup Predicted and Observed in May 2018

A SOZ (*Sistema Obespecheniya Zapuska*) ullage motor, or SL-12 auxiliary motor, from a Proton Block DM fourth stage fragmented at 2:06Z on 22 May 2018. These motors have a long history of fragmentations, this event being the 48th breakup of this class of object over its program history and the first since September 2017. A total of 380 SL-12 Auxiliary Motors were cataloged between 1970 and 2012, of which 64 remain on orbit as of 8 August 2018. Of these 64, 35 are now believed to be intact. The remaining 29 have fragmented and remain on-orbit while an additional 20 fragmented parent bodies have reentered.

Ullage motors, used to provide three-axis control to the Block DM during coast and to settle propellants prior to an engine restart, were routinely ejected after the Block DM stage ignited for the final time. The reader is referred to a prior ODQN (ODQN, Vol. 18, Issue 4, pp. 1-2) for an illustration and engineering drawing of a typical SOZ unit.

This SOZ unit (International Designator 2010-007H, U.S. Strategic Command [USSTRATCOM] Space Surveillance Network [SSN] catalog number 36407) is associated with the launch of the Cosmos 2459-2461 spacecraft, members of the Russian global positioning navigation system (GLONASS) constellation. Its sister unit, International Designator 2010-007G, SSN #36406, had previously fragmented on 9 July 2014 and was reported in the cited ODQN.

The motor was in a highly elliptical 18929- x 602-km altitude orbit at an inclination of 65.1° at the time of the breakup; the event is estimated to have occurred at an altitude of approximately 13745.8 km at a latitude of 8.6° South and longitude of 90.0° East. The unit fragmented into over 60 pieces, but due to difficulties in tracking objects in deep space elliptical orbits, this event may have produced many more fragmentation debris than have been observed to date. Catalog interpretation is complicated somewhat by the presence of three payloads, the third and fourth stage rocket bodies, the so-called "SL-12 PLAT" (the "platform," in reality a stage casing), mission-related debris, debris from the 2016 fragmentation of the ullage motor -007G, and the presence of an unknown number of debris associated with -007H entering the public catalog. The mission related debris, long decayed from orbit, is piece tags J-L. Piece tags M-W (SSN #41695-41704) inclusive entered the catalog between 12 and 28 July 2016, so are associated with the sister motor -007G. However, piece tags X-AA (SSN #43525-43528) inclusive entered the catalog between 29 June and 9 July 2018 as "SL-12 DEB" while piece tags AB-AG (SSN #43542-43545, 43579, and 43580) inclusive entered the catalog between 9 and 22 July 2018 as "SL-12 R/B (AUX MOTOR) DEB". Time could not be used to differentiate debris between -007G and -007H in this case, so the evolution of the fragment right ascension of ascending nodes was examined to determine the identity of the parent body and any significance of the catalog common names. This analysis indicated that 10 pieces of debris, piece tags X-AG inclusive, appear to be associated with -007H. Additional debris may enter the catalog over time.

This event represents the third SOZ unit fragmentation predicted by analysts of the Air Force Space Command 18th Space Control Squadron [1]. Their analysis indicates that SOZ units experience outgassing prior to the fragmentation event; the main body of the SOZ can then exhibit the effects of outgassing for several days after the event. This new analytical technique is useful in prompting additional surveillance of a SOZ unit prior to and post-fragmentation and assessing event time for modeling and risk assessment purposes.

Reference

1. Slatton, Z., and McKissock, D. "Methods of Predicting and Processing Breakups of Space Objects," Presented at the 7th European Conference on Space Debris, Darmstadt, Germany, (2017). ♦

Space Debris Sensor On-orbit Status

The Space Debris Sensor (SDS), a Class 1E technical demonstrator payload, was robotically installed and activated aboard the International Space Station's *Columbus* module on 1 January 2018. As reported previously (ODQN vol. 22, Issue 2, May 2018, p. 1), SDS suffered a failure to recover telemetry on 26 January at approximately 0330 GMT. During its January operations, SDS had regularly experienced partial software lockups and failed to accept commanding or send data over its 1553 standard low data-rate channel (data on the ISS LAN Ethernet medium data-rate channel was unaffected); termed Anomaly 1 by the SDS Engineering and Operations (Ops) teams, the payload could be recovered by cycling operational power. This was facilitated by NASA Marshall Space Flight Center/ Payload Operations and Integration Center (POIC) and ESA colleagues. Anomaly 2, associated with the 26 January event, resulted in complete loss of telemetry and command capability.

The SDS teams launched activities to address and resolve Anomaly 1 during SDS' January operations, and to resolve both anomalies after 26 January. These included in-depth analysis of SDS engineering (health and status, or "housekeeping" data), science data, and associated SDS and ISS telemetry streams and measured state variables. Hypotheses were developed and when possible, evaluated on the SDS Ground Unit. As part of this diagnostic and recovery effort, a formal fault tree methodology was adopted, and lessons learned documentation implemented. These formal engineering analysis efforts examined both SDS hardware and software, and identified a primary expected condition aboard the SDS control computer's corrupted startup and/or application files; other possible but recoverable conditions; and unrecoverable conditions. SDS teams developed procedures to address the most likely condition and tested the prime recovery procedure at the NASA Sonny Carter Training Facility's Joint Station LAN facility and the POIC, completing ground-based preparations with a full-up simulation of the recovery in early April.

continued on page 3

SDS On-orbit Status

continued from page 2

A prime recovery method attempt failed in late April for reasons unconnected to SDS or the method. A secondary recovery method, switching SDS power feeders aboard the *Columbus* module, was conducted in early June with no success. The prime recovery method was attempted again in late June. While the ISS telemetry link-state variable indicated connectivity with SDS, the SDS was not discoverable on the ISS network and the process was terminated. All identified recovery options have been implemented and attempted; no further recovery attempts are planned or scheduled.

At the current time, the SDS Engineering and Ops teams are engaged in finishing out the fault tree and lessons learned documentation, and the Ops team is refocusing toward analyzing both engineering and environmental data and the science contained in the over 1300 acoustically-triggered events. We anticipate presenting results and outcomes in appropriate fora, proceedings, and journals. ♦

Spacecraft Material Ablation Testing at UT Austin

The NASA Orbital Debris Program Office (ODPO) portfolio of responsibilities includes myriad topics associated with orbital risk and reentry safety. One topic is end of mission (EOM) satellite atmospheric reentry, and the potential human casualty risk due to hardware surviving the thermal loads generated during reentry. Several strategies are employed to mitigate this risk; however, there is also significant incentive for ODPO to develop a deeper understanding of the physics of satellite breakup during reentry. The ODPO has recently teamed with the Johnson Space Center's Structural Engineering Program and the University of Texas at Austin (UT Austin) to test common composite materials. The goal is to develop a better understanding of how these materials respond in a representative thermal loading environment.

The first phase of the test series was completed during the week of 23-27 April 2018 when several modern materials were tested in the UT Austin Inductively Coupled Plasma Torch. The torch can simulate entry temperature and heat flux, and oxygen flux, but not the near-vacuum conditions and supersonic conditions of an arc-jet facility. Because it operates in a shirt-sleeve laboratory environment, samples can be loaded and tested in mere seconds-to-minutes.

Design engineers increasingly rely on composite materials such as glass fiber-reinforced polymers and carbon fiber-reinforced polymers in spacecraft design. Recent testing will be used to characterize material response phenomena as well as to identify testing needed in future phases of the series. Future testing provides an opportunity to collect higher fidelity data needed to build improved material models. When completed, this test series will improve modeling assumptions and characterize improved material models, thereby increasing the accuracy of reentry analysis software used by the ODPO to assess casualty risks for reentering satellites. ♦

a) Epoxy phase change from solid with volatiles charring and burning.

b) Carbon filament erosion starts; epoxy has been almost completely removed.

c) Carbon filaments have eroded, exposing aluminum honeycomb to plasma.

d) Aluminum honeycomb burns, leading to complete demise of structural panel.

Progression to demise of a carbon fiber and aluminum honeycomb panel in ICP thermal environment. Credit: NASA ODPO

SUBSCRIBE to the ODQN or UPDATE YOUR SUBSCRIPTION ADDRESS

If you would like to be notified when a new issue of the ODQN is published or have already subscribed but no longer receive email notifications, please update your email address using the ODQN Subscription Request Form located on the NASA Orbital Debris Program Office (ODPO) website at https://orbitaldebris.jsc.nasa.gov. You can access this form by clicking first on the "Quarterly News" tile, then selecting the navigation link within the sentence "to be notified by e-mail...".

PROJECT REVIEW

NASA ODPO's Large Constellation Study

J.-C. LIOU, M. MATNEY, A. VAVRIN,
A. MANIS, AND D. GATES

In recent years, several commercial companies have proposed telecommunications constellations consisting of hundreds to thousands of 100-to-300-kg class spacecraft in low Earth orbit (LEO, the region below 2000-km altitude). If deployed, such large constellations (LCs) will dramatically change the landscape of satellite operations in LEO. Fig. 1 shows the current mass distribution in LEO. The top blue histogram shows the total and the three curves below show a breakdown by object type (spacecraft, rocket bodies, or other). The mass distribution is dominated by spacecraft and upper stages (*i.e.*, rocket bodies). The yellow bars from 1100 km to 1300 km altitudes show the notional mass distribution from 8000 150 kg LC spacecraft or, equivalently, 4000 300 kg LC spacecraft. From the large amount of mass involved, it is clear that the deployment, operations, and frequent de-orbit and replenishment of the proposed LCs could significantly contribute to the existing orbital debris problem.

To better understand the nature of the problem, the NASA Orbital Debris Program Office (ODPO) recently completed a parametric study on LCs. The objective was to quantify the potential negative debris-generation effects from LCs to the LEO environment and provide recommendations for mitigation measures. The tool used for the LC study was the ODPO's LEO-to-GEO Environment Debris (LEGEND) numerical simulation model, which has been used for various mitigation and remediation studies in the past [1, 2]. For the LC study, more than 300 scenarios based on different user-specified assumptions and parameters were defined. Selected results from key scenarios are summarized in this article.

The LEO Environment without Large Constellations

To establish a benchmark to assess the effects from LCs, several baseline scenarios were completed first. Fig. 2 shows the environment projection without LCs. The historical curve reflects the documented launches and breakup events between 1957 and 2015. The antisatellite test conducted by China and the accidental collision between Iridium 33 and Cosmos 2251 were the reasons for the jump in 2007 and 2009, respectively. Future launch traffic is a repeat of the launches over the last 8 years of the historical space activities (2008-2015). The environment is projected 200 years into the future, through the year 2215.

Each future projection curve is the average of 100 LEGEND Monte Carlo (MC) simulation runs. The top red curve is the result of a non-mitigation scenario where LEO-crossing upper stages and spacecraft are left at mission altitudes at the end of mission operations rather than conducting postmission disposal (PMD) maneuvers to lower their orbits to follow the 25-year decay rule. Upper stages and spacecraft are also assumed to explode in the future with accidental explosion probabilities derived from the historical explosion events. The middle black-dashed curve is the result of a scenario where LEO-crossing upper stages and spacecraft are assumed to follow the 25-year decay rule at the end of their missions with a PMD reliability of 90%. The bottom blue-dotted curve is the result of a scenario where, in addition to the 90% PMD success rate, no explosions occur in the future.

As expected, the non-mitigation scenario leads to a rapid LEO population increase over time, with an approximately 330% increase in 200 years, *i.e.*, from the beginning of 2016 to the end of 2215. The non-linear increase is also an indication of the collision feedback effect in the environment. With a global 90% PMD implementation of the 25-year decay rule, however, the debris population growth is reduced to about a 110% linear increase in 200 years. If explosions can be eliminated, the population growth is further reduced to 40% in 200 years.

Fig. 3 shows the cumulative numbers of catastrophic collisions involving 10 cm and larger objects over time. A catastrophic collision occurs when the ratio of impact kinetic energy to target mass exceeds 40 J/g. The outcome of a catastrophic

continued on page 5

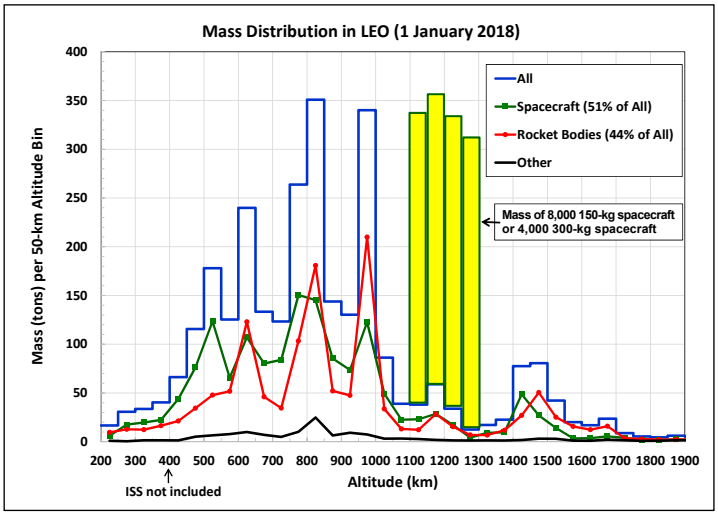

Figure 1. Mass distribution in the current LEO environment. The blue histogram is the total and the population breakdown is shown in red (rocket bodies), green (spacecraft), and black (others). The yellow bars between 1100 km and 1300 km shows the notional mass distribution from 8000 150 kg spacecraft or, equivalently, 4000 300 kg spacecraft.

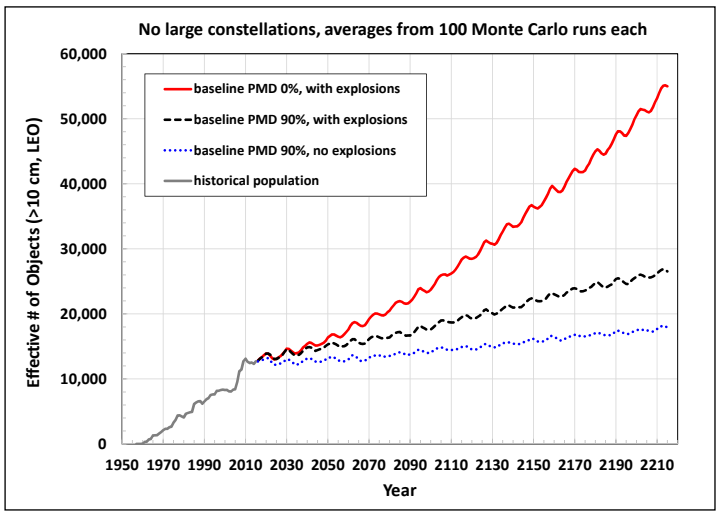

Figure 2. LEGEND-simulated historical LEO environment and results from three different future projection scenarios. Each projection curve is the average of 100 MC runs. The effective number is defined as the fractional time, per orbital period, an object spends between 200 km and 2000 km altitudes.

Large Constellation Study

continued from page 4

collision is the total fragmentation of the target, whereas a non-catastrophic collision only results in minor damage to the target and generates a small amount of debris that should have negligible contribution to the long-term debris population increase. Again, the non-mitigation scenario leads to a non-linear increase of catastrophic collisions, a total of 61 in 200 years, whereas the effective implementation of PMD and additionally, elimination of future explosions can reduce the numbers of catastrophic collisions to 27 and 21, respectively, in 200 years. The increases in effective number of objects and catastrophic collisions for the 90% PMD scenarios, with future explosions, are used to benchmark the effects when LCs are added to the simulated environment as described in the sections below.

The LEO Environment with Large Constellations – PMD Reliability

All LC scenarios assume that, in addition to the background (BG) future launch traffic cycle shown in Fig. 1, three LCs operate from 1000- to 1325-km altitudes with different inclinations and orbital planes. The first set of scenarios assumes a total of 8300 spacecraft from the 3 constellations. The masses of individual spacecraft are 150 kg for constellations A and B, and 300 kg for constellation C. Each spacecraft is deployed at 500-km altitude, raises its orbit to mission altitude, operates for 5 years, then conducts PMD operations to lower its orbit such that it will naturally decay in 5 years. Then, the spacecraft is replaced by a new one. Furthermore, it is assumed that conjunction assessments and collision avoidance maneuvers are conducted for LC spacecraft that have successful deployment, operations, and PMD through final reentry.

Results from the first set of LC scenarios, where LCs maintain full operations with regular spacecraft replenishment for 20 years, are shown in Fig. 4. Accidental explosions are assumed for the LC spacecraft. The accidental explosion probability for each LC spacecraft is 0.001 over a 5-year mission life. The black-dashed curve from Fig. 1 (BG PMD 90% with accidental explosions) is also included for comparison. For the LC PMD 90% scenario, the additional debris population increase with respect to the BG population (the black-dashed curve) is approximately 290% in 200 years. Even with a 95% PMD for the LC spacecraft, the additional population increase is still close to 100%. When the LC spacecraft PMD success rate is increased to 99%, the additional population increase is reduced to 22%.

The cumulative numbers of catastrophic collisions are shown in Fig. 5. The LC PMD 90% scenario leads to a non-linear increase for a total of 260 catastrophic collisions in 200 years. For LC PMD 95%, the total number of catastrophic collisions is 90 in 200 years, equivalent to one catastrophic collision every 2.2 years. Since most of these predicted catastrophic collisions occur between 1000- and 1300-km altitudes, the

continued on page 6

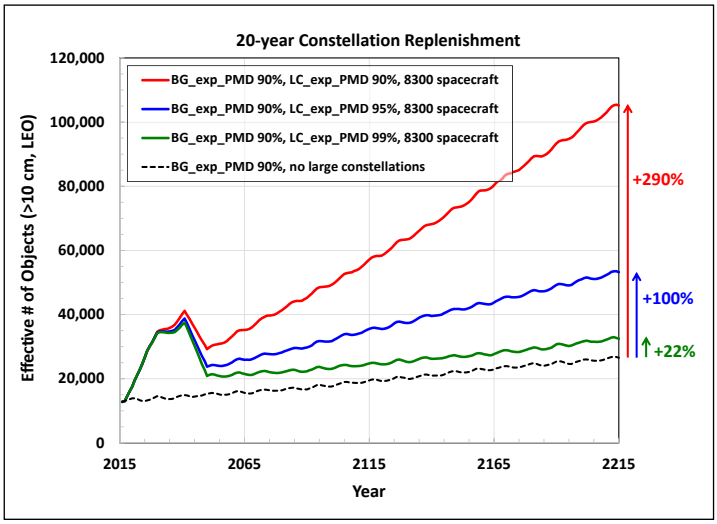

Figure 4. Results from LC scenarios where the LCs maintain full operations with spacecraft replenishment for 20 years. The total number of spacecraft in 3 LCs is 8300. The differences between the top three curves and the black-dashed curve in 2215 are +290% (red), +100% (blue), and +22% (green), respectively.

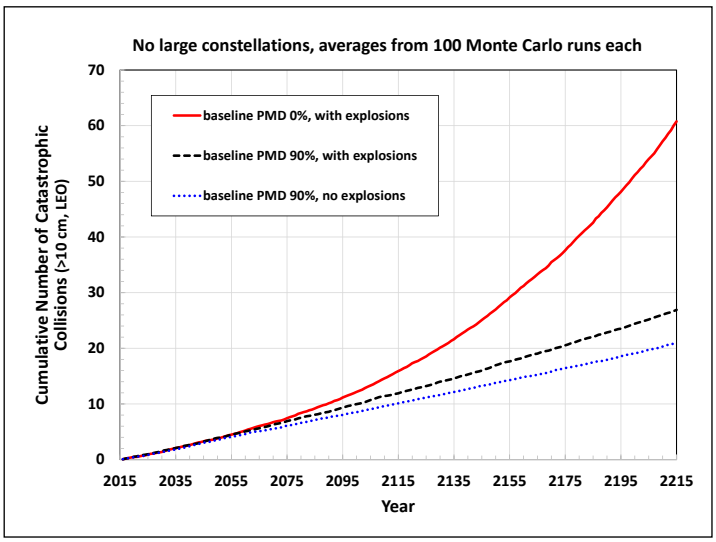

Figure 3. LEGEND-simulated cumulative numbers of catastrophic collisions over time.

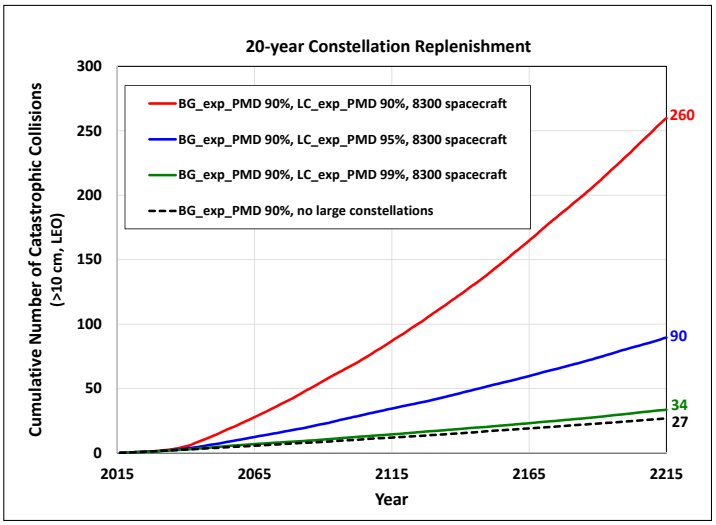

Figure 5. Results from LC scenarios where the LCs maintain full operations with spacecraft replenishment for 20 years. The total number of spacecraft in 3 LCs is 8300. The total numbers of catastrophic collisions in 200 years for the 4 curves are (top to bottom) 260, 90, 34, and 27, respectively.

Large Constellation Study

continued from page 5

generated fragments could seriously threaten the safe operations of LCs in the region. If the LC PMD is increased to 99%, the number of catastrophic collisions is limited to 34 in 200 years, which is very close to the total of 27 for environment projection without LCs.

The need for LCs to follow a high PMD success rate is further illustrated in Fig. 6 where the operations and routine spacecraft replenishment of the three LCs are assumed to continue for 50 years. For this set of scenarios, the total number of spacecraft from the 3 LCs is reduced to 6700 spacecraft. The accidental explosion probability for each LC spacecraft is also 0.001 over a 5-year mission life. The additional debris population increases in 200 years for the LC scenarios with PMD 90%, 95%, 99%, and 99.9% are +590%, +180%, +40%, and +27%, respectively, with respect to the BG population. The cumulative numbers of catastrophic collisions in 200 years are shown in Fig. 7. Even with an LC PMD of 95%, there is a non-linear increase for a total of 158 catastrophic collisions in 200 years, equivalent to one catastrophic collision every 1.3 years. If the LC spacecraft can achieve PMD 99%, the number of catastrophic collisions is limited to 40 in 200 years. The further increase in LC spacecraft PMD reliability to 99.9% has some additional but minor benefits.

The LEO Environment with Large Constellations – Accidental Explosion Probability

The third set of scenarios assesses the effects of accidental explosion probabilities of the LC spacecraft to the environment. The total number of spacecraft in the 3 LCs is 6700, the operations and routine spacecraft replenishment of the three LCs are assumed to continue for 50 years, and the LC PMD success rate is set to 90%. The accidental explosion probabilities (Pexp) of LC spacecraft are set to 0.01, 0.001, 0.0001, and 0, respectively, over the 5-year mission lifetime for the four scenarios. The projected population increase in 200 years is shown in Fig. 8. For comparison, the no-large-constellations projection (*i.e.*, the black-dashed curve from Fig. 1) is included also.

The combination of 90% PMD success rates and accidental explosion probabilities of 0.01 for LC spacecraft leads to a more than tenfold increase of the debris population in 200 years (top red curve). When the accidental explosion probabilities of the LC spacecraft are reduced to 0.001, the population growth is approximately cut in half. Further reduction in the accidental explosion probabilities only leads to a minor improvement. This is also evident in Fig. 9 where the distribution of objects, as a function of altitude, at the end of the 200-year projection (the year 2215) is shown. Relative to the environment projection without large constellations, there is a two-to-three orders of magnitude debris population increase between 1000 km and 1200 km altitudes. For the accidental explosion probability effect, the largest improvement is from 0.01 to 0.001 over 5-year mission time. Once the probability is limited to 0.001, the debris population increase is primarily driven by the 90% PMD success rate of the LC spacecraft for the scenarios shown in Figs. 8 and 9. If the LC spacecraft can achieve 99% PMD reliability and 0.001 accidental explosion probabilities, their contribution to the future debris environment appears to be limited and acceptable, as shown by the green curves in Figs. 6 and 7.

Summary

Achieving high PMD reliability for LC spacecraft requires several elements. The first is the quality of the spacecraft's design and fabrication, especially the key subsystems needed to maintain spacecraft health and operations from

continued on page 7

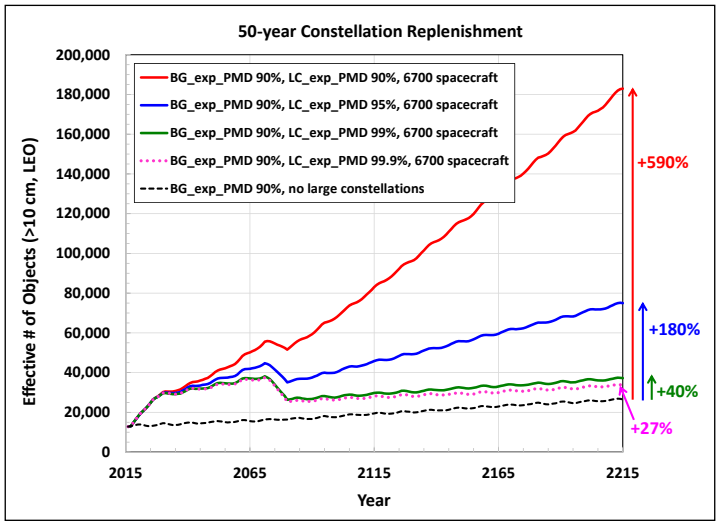

Figure 6. Results from LC scenarios where the LCs maintain full operations with spacecraft replenishment for 50 years. The total number of spacecraft in 3 LCs is 6700. The differences between the top four curves and the black-dashed curve in 2215 are +590% (red), +180% (blue), +40% (green), and +27% (purple-dotted), respectively.

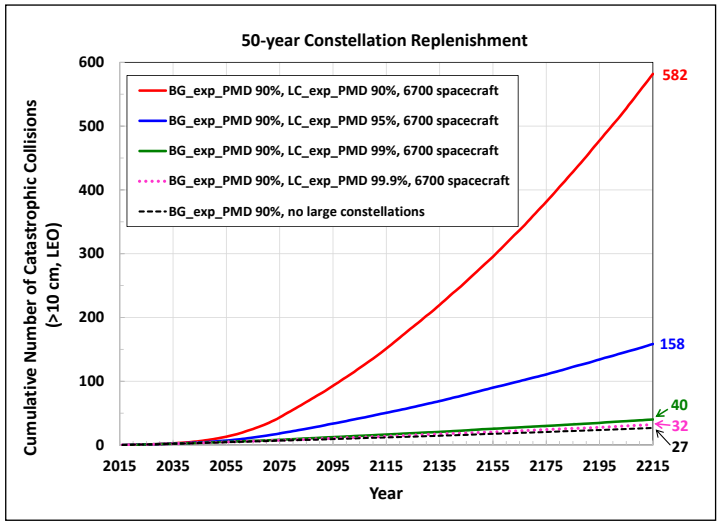

Figure 7. Results from LC scenarios where the LCs maintain full operations with spacecraft replenishment for 50 years. The total number of spacecraft in 3 LCs is 6700. The total numbers of catastrophic collisions in 200 years for the 4 curves are (top to bottom) 582, 158, 40, 32, and 27, respectively.

Large Constellation Study

continued from page 6

deployment, through operations, then to successful PMD maneuvers at the end of mission. The second is the allocation of sufficient resources/fuel needed to sustain mission operations, including PMD maneuvers. The third is the implementation of adequate micrometeoroid and orbital debris (MMOD) impact protection for subsystems needed to maintain mission operations and conduct PMD maneuvers. Because of the weak atmospheric drag above 1000 km altitude, defunct spacecraft in that region have orbital lifetimes on the order of thousands of years or longer. They are a danger to the operations of LCs and more importantly, are a long-term threat to the LEO environment—defunct spacecraft can and will collide with other debris over time, increasing the potential of generating more debris to trigger a collision cascade effect in the region.

The only option to address the problem of defunct LC spacecraft is active debris removal, which by itself, is a challenge in technical readiness, operations, and cost. Based on results from the parametric study, a 99% spacecraft PMD reliability is needed to mitigate the serious long-term debris generation potential from LCs similar in scope to the study scenarios. For MMOD impact protection, the NASA orbital debris requirement to limit the probability of accidental collisions with small MMOD to ensure successful PMD operations to 0.01 also appears to be necessary for the LC spacecraft [3].

One can certainly make an argument that limiting accidental explosion probabilities is part of PMD reliability. Historically, however, due to the dominance of explosion fragments in the environment and the immediate threat from the generated fragments to other operational spacecraft, this aspect of orbital debris mitigation has been treated separately from PMD [4]. More than 170 accidental explosions have been documented since 1957 and many of them occurred years after the end of mission operations. Since the spacecraft in the same LC are likely to share similar, if not identical, designs and fabrication processes, a potential flaw leading to explosions can exist in many spacecraft and may not be identified until years after launch or operations in orbit. Based on the parametric study results, it is necessary to limit the probability of accidental explosions for the LC spacecraft during mission operations to less than 0.001, which is consistent with the NASA orbital debris requirement to limit accidental explosions [3].

One of the assumptions of this LC study is that launch vehicle upper stages will deploy the LC spacecraft near 500 km and let the spacecraft raise their own orbits to mission altitudes above 1000 km. Because of the short orbital lifetimes of the upper stages from 500 km (approximately 5 years or less), they don't contribute to the long-term orbital debris problem. If the upper stages are to deploy the LC spacecraft at higher altitudes, then orbital debris mitigation for the upper stages will need to be addressed as well.

References

1. Liou, J.-C. and Johnson, N.L. "Risks in space from orbiting debris," *Science* 311, pp. 340-341, (2006).
2. Liou, J.-C. "An active debris removal parametric study for LEO environment remediation," *Adv. Space Res.* 47, pp. 1865-1876, (2011).
3. NASA Technical Standard, Process for Limiting Orbital Debris, NASA-STD-8719.14A (2012).
4. U.S. Government Orbital Debris Mitigation Standard Practices, February 2001. Available at https://orbitaldebris.jsc.nasa.gov/library/USG_OD_Standard_Practices.pdf).

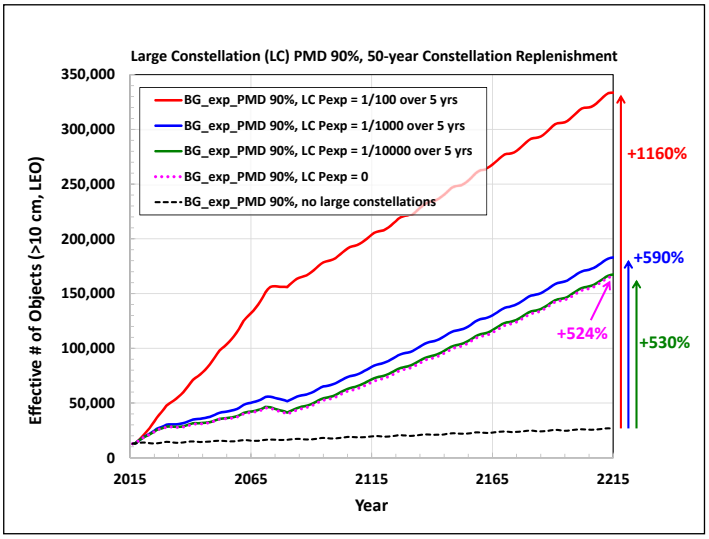

Figure 8. Results from LC scenarios where the LCs maintain full operations with spacecraft replenishment for 50 years. The total number of spacecraft in 3 LCs is 6700. The LC PMD is set to 90%. The differences between the top four curves and the black-dashed curve in 2215 are +1160% (red), +590% (blue), +530% (green), and +524% (purple-dotted), respectively.

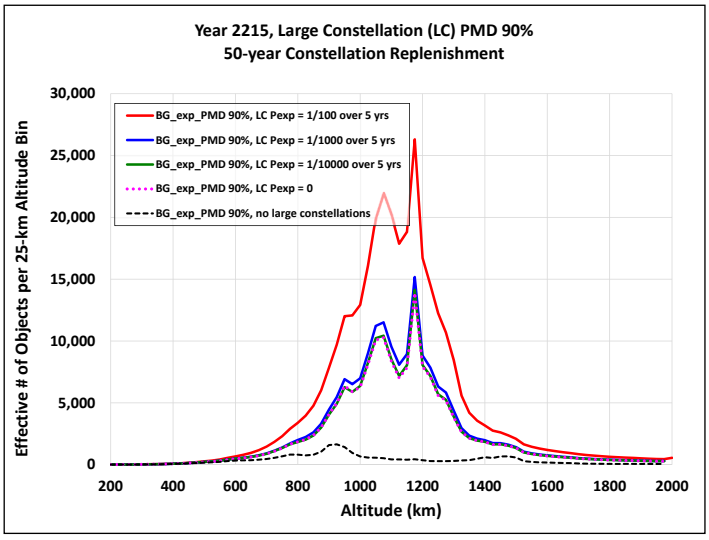

Figure 9. Distribution of the debris populations as a function of altitude at the end of the 200-year projection (the year 2215) from the scenarios shown in Fig. 8.

ORDEM Interpolation—a Review and Prospectus

P. ANZ-MEADOR AND M. MATNEY

The Orbital Debris Engineering Model (ORDEM) v. 3.0 introduced many new capabilities and features as it supplanted its predecessor model, ORDEM 2000; however, a subtle feature that may escape the immediate attention of many users is the method of interpolating between the 11 reference points distributed in half-decade intervals in $\log_{10}$(size) space between the ORDEM minimum debris size (10 μm) and its maximum size (1 m)—a total of five orders of magnitude in debris characteristic size. Orbital debris flux changes over many orders of magnitude as a function of size, and the standard way to handle this dynamic distribution is to interpolate the log-log distribution.

A fundamental representation of the debris number or flux is to give the value for a given size or larger. This cumulative distribution dates to the earliest days of micrometeoroid and orbital debris studies, under the assumption that if an object of a certain size poses a penetration risk to a target spacecraft, *i.e.*, the critical diameter, then all larger sizes pose that same penetration risk. While interpolation may seem cosmetic in nature when applied to the entire flux-as-a-function-of-size curve, in which all half-decades are filled to some degree, it is crucially important when determining the flux corresponding to the estimated critical diameter for a given ORDEM subpopulation at a given orientation and relative velocity with respect to a target. This is a requirement for using ORDEM outputs in risk estimation codes such as NASA's BUMPER series of codes.

Thus, a robust interpolator that preserves the cumulative nature of the function is an absolute requirement. Other considerations are the ability to handle discontinuities and the representation of zero in $\log_{10}$(flux) space. An example of the former is the ORDEM low-density (LD) population transition at 1 mm size. For a given azimuth-elevation-relative velocity bin, there may be a nonzero LD flux for sizes larger than 1 mm, but for smaller sizes, the model does not include any further flux, based on the paucity of evidence found for LD debris in examinations of the Shuttle window and radiator cratering record. This decision manifests itself as a flat line in cumulative distributions for sizes less than 1 mm. Similarly, the azimuth-elevation-relative velocity bins for many populations have sizes where the flux drops to zero. In the half-decade between the last non-zero flux and the first zero flux, a very steep slope may be encountered, even allowing for an approximation of zero flux by a very small number, say -30, in $\log_{10}$(flux) space.

Prior interpolation schemes were developed in-house at the NASA Orbital Debris Program Office (ODPO). In assessing the make-or-buy decision for ORDEM 3.0, however, the government off-the-shelf (GOTS) software embodied in the Piecewise Cubic Hermite Interpolating Polynomial (PCHIP) package, developed by the U.S. Department of Energy, was chosen. Among the reasons motivating this choice was that PCHIP was a validated code, met all numerical requirements in handling cumulative data sets and error case handling, and could be distributed bundled with the ORDEM 3.0 executable package. PCHIP performance for a challenging data set is portrayed in Fig. 1, where the interpolator handles the transitions between flat sections (size ranges with no modeled populations) with size ranges with rapidly varying flux. Following PCHIP implementation in the ORDEM release package, the NASA BUMPER code was modified to use an equivalent, publicly-available version of the PCHIP interpolator and its implementation verified.

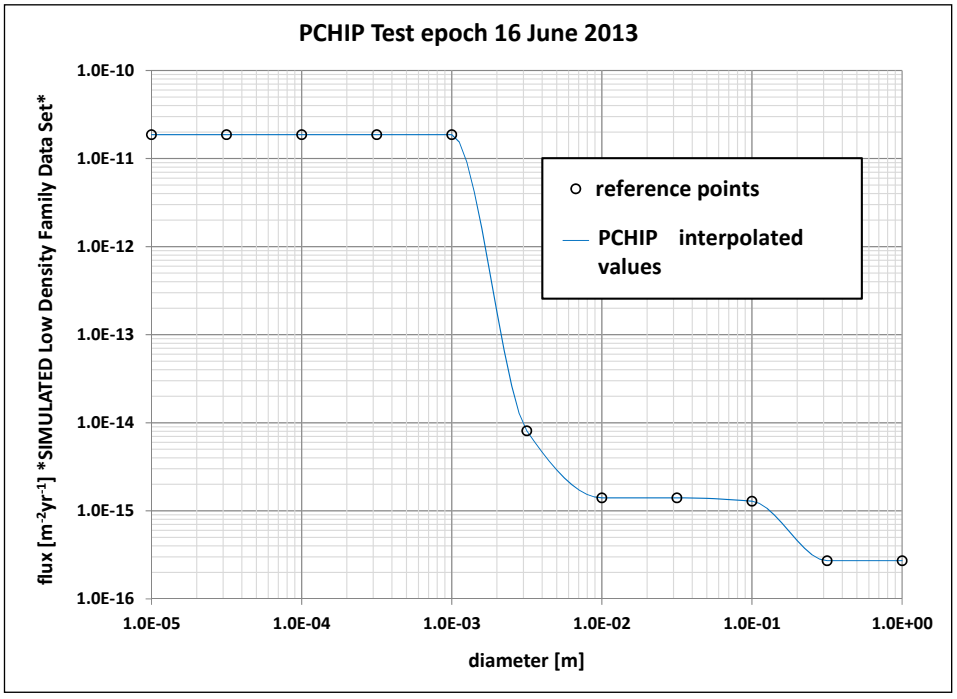

Figure 1. PCHIP implementation for a challenging data set, indicated by 11 half-decadal reference points in $\log_{10}$(size) space. Five hundred interpolated points provide a smoothly interpolated curve over this data set. A simulated low-density data set is defined by the reference points.

Figure 2 illustrates the critical function of PCHIP—interpolating a flux associated with a critical diameter—for ORDEM subpopulations. In this exemplar, the 2019 flux on a spacecraft in an 841 km x 856 km altitude, 98.8° inclination orbit is portrayed by solid or open markers (11 reference points per subpopulation) and the 101 point over five size decades interpolation by solid or dotted lines. Critical diameters for penetration of an Aluminum Whipple shield [1] are indicated by heavy open circles for the LD, medium density (MD), high density (HD), Sodium-Potassium (NaK) reactor coolant droplets, and Intact populations (note that this latter population is only modeled down to 10 cm characteristic lengths and represents the cataloged on-orbit intact population).

This set of five subpopulations is drawn from the ORDEM output for a single case of azimuth, elevation, and relative velocity with respect to the target spacecraft. Note that critical diameters vary by the mass density attributed to each of the five subpopulations. Note also that in the half decade between the last non-zero flux value and the first significant zero, the current implementation of the PCHIP tool adds 8 additional reference points, in addition to the 11 reference points produced by ORDEM, to steer the distribution; these may be seen for the HD and NaK subpopulations in the half-decade between 3.16 and 10.0 cm.

Since its release, concerns have arisen over risk estimates when interpolators other than PCHIP are used to estimate critical diameters in ORDEM subpopulations. This outcome is most common when comparing BUMPER results to results generated by other risk estimators, including ESABase. This is not a surprising

continued on page 9

ORDEM Interpolation

continued from page 8

outcome, particularly when critical diameters reside in portions of the flux curve that are rapidly changing. Two different interpolation schemes are likely to produce dissimilar results, particularly in dynamic regions.

A further difference has been noted in comparisons between the output of the released version of ORDEM, where the software sums the five ORDEM subpopulations at the 11 reference points, then interpolates; and BUMPER 3, where the interpolation is applied to each subpopulation for a given azimuth, elevation, and relative velocity separately, then summed. In certain size regimes, differences can be significant. The BUMPER 3 procedure is considered to be the correct one, and the upcoming release of ORDEM 3.1 will rectify this difference by interpolating the subpopulations and then summing the result in the manner of BUMPER 3. In addition, the ODPO anticipates removing the steering function due to the robust nature of the PCHIP interpolator. This function was a legacy of prior interpolation functions but is no longer deemed necessary.

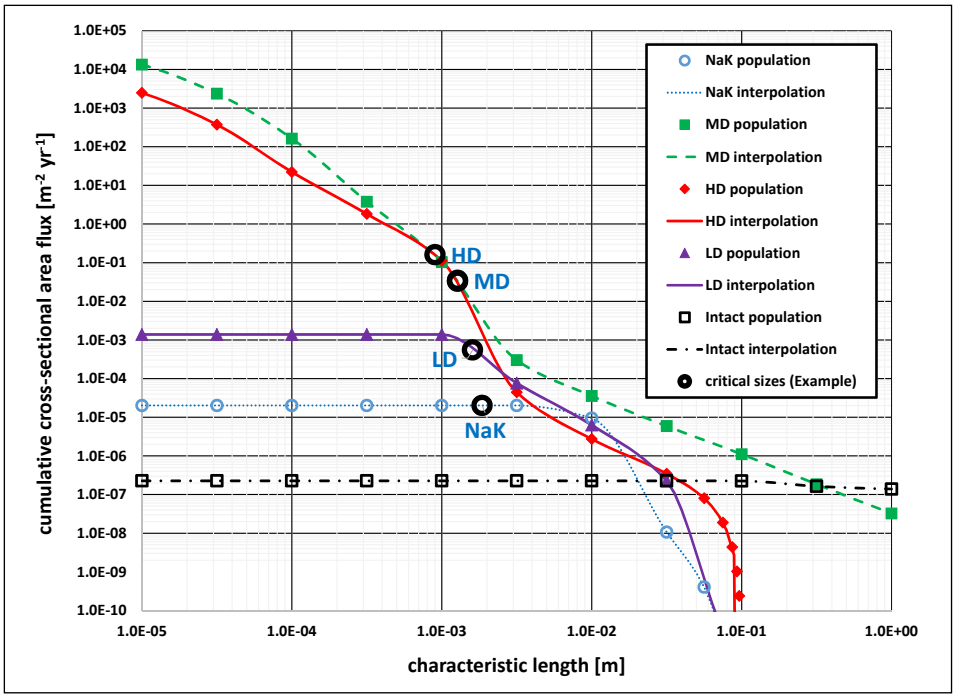

Figure 2. PCHIP interpolation of ORDEM subpopulations, with critical diameters required to penetrate an Aluminum Whipple bumper indicated. Interpolation is required to assess the subpopulation flux at the computed critical diameters. Critical diameters vary according to mass density of the debris projectile; for this evaluation, mass densities of 0.9 (NaK), 1.4 (LD), 2.8 (MD), 7.9 (HD), and 2.8 (Intacts) g/cm^3 were used. See text for specifics of the 2019 sun-synchronous target orbit for this example.

Reference

1. Christiansen, E.L., "Shield Sizing and Response Equations", NASA-TM-105527 (1991).

♦

Orbital Debris Analyst: First in the Series

This feature will examine complex debris clouds—those that contain more than one component for a given launch or international designator; future features may examine multiple event debris clouds. As related in the lead news article this issue, both of the 2010-007 SOZ ullage motors have now fragmented, as has occurred with other launches of the Soviet/Russian Global Navigation Satellite System (GLONASS), *e.g.*, 2008-067. The problem at hand is understanding and properly accounting for the objects associated with each object in the public catalog. While the contents of that catalog are insufficient to distinguish between the two distinct fragmentation event fragments, the Two-Line Element (TLE) sets provide orbital information that may be used to differentiate the two clouds. TLE sets are available at https://www.space-track.org/. In the cited case, the concern is that fragments of the -007G motor entered the catalog interspersed with fragments of the -007H motor. The differential precession of the right ascension of ascending node was plotted as a function of time to spatially

continued on page 10

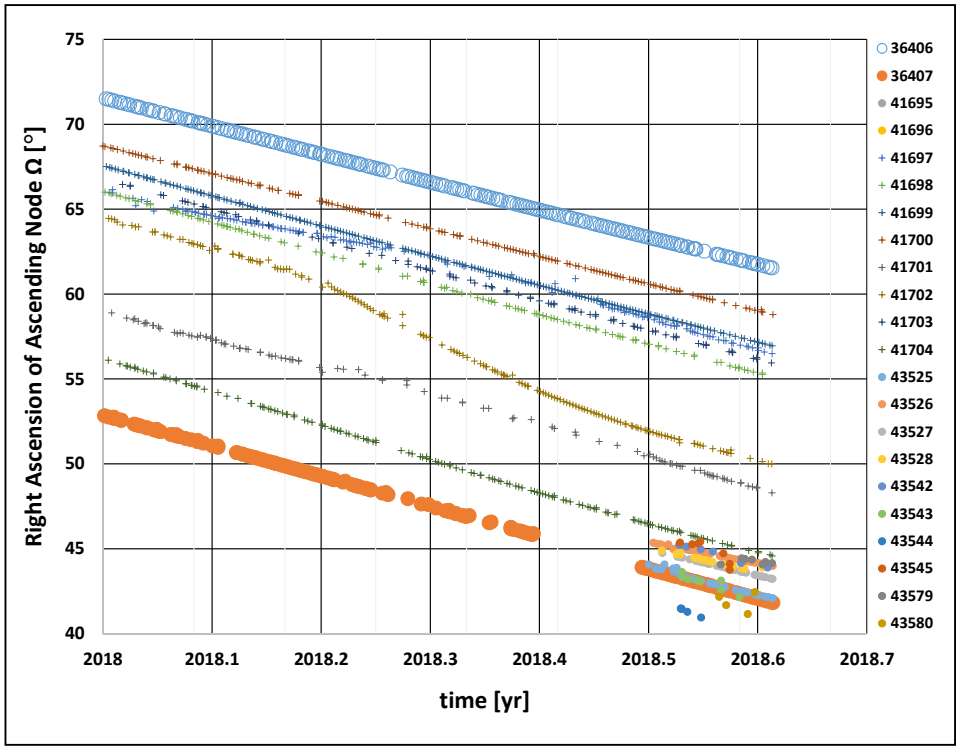

OD Analyst

continued from page 9

separate the members of the -007H (May 2018 event) and -007G (July 2014 event) clouds.

All objects identified as fragmentation debris are plotted, though the right ascension of some objects may be larger than 75° and hence off the plot. Parent bodies are indicated by circles (open for -007G, closed for -007H) and fragments by "+" (-007G) or circles (-007H), both assessments being predicated upon the analysis. This plot clearly indicates that 2010-007 piece tags X through AG, inclusive, are associated with the -007H event. ♦

CONFERENCE AND WORKSHOP REPORTS

The SIAM Conference on Uncertainty Quantification (UQ18), 16-19 April 2018, Garden Grove, California

The 2018 Society of Industrial and Applied Mathematics (SIAM) Conference on Uncertainty Quantification was held from 16-19 April in Garden Grove, California, with about 600 participants from the global statistics and applied math community. This year's conference was hosted by the SIAM Activity Group on Uncertainty Quantification, and consisted of 164 sessions, tutorials, and special talks. Topics included model reduction, sensitivity analysis, data assimilation, experimental design, and applications to specific problems.

This meeting report includes conference highlights, with emphasis on presentations relevant to ODQN readers. The first day featured presentations on modeling and data assimilation with uncertainty and random noise, as well as a featured plenary presentation titled "Scalable Algorithms for PDE-Constrained Optimization Under Uncertainty." Day two included sessions on computer implementations of uncertainty models, numerical analysis, surrogate modelling, and use of extreme-scale parallel computing. The featured plenary presentation was "Model Uncertainty and Uncertainty Quantification."

Day three continued with sessions on Bayesian statistical methods, high-performance computing, and dimension reduction for large-scale problems. Another invited talk was on "Multi-level and Multi-index Monte Carlo Methods in Practice." The final day concluded with an invited talk titled "Multilevel Markov Chain Monte Carlo Methods for Uncertainty Quantification," which discussed methods to reduce computational cost of evaluating models while maintaining high accuracy. Selected special presentations and invited talks were available at: https://www.pathlms.com/siam/courses/7376. ♦

The 5th European Workshop on Space Debris Modeling and Remediation, 25-27 June 2018, CNES HQ, Paris

The Centre National d'Études Spatiales (CNES) Headquarters hosted the biannual 5th European Workshop on Space Debris Modeling and Remediation 25-27 June 2018. In nine oral presentation sessions and a poster presentation, researchers from academia, commercial enterprises, and government institutes and agencies presented their findings and recommendations on many aspects of orbital debris modeling and environmental remediation technologies and processes. The sessions were thematically arranged as modeling for stability; economic and legal aspects; remediation solutions; modeling mitigation strategies and outcomes; attitude dynamical modeling; orbital dynamical modeling; laser applications for remediation; modeling end-of-life phenomena, including reentry; and remediation technologies. The breadth of the workshop prevents a review of all papers and posters, but select topics are summarized here.

Highlights of the modeling-related sessions include presentations on the NASA Orbital Debris Engineering Model (ORDEM) version 3.1 (NASA), the Space Objects Long-term Evolution Model (SOLEM; the People's Republic of China), and the European ReDSHIFT modeling environment. Multiple presentations over the 3-day workshop featured various aspects of the project, including results to date of ground-based Design for Demise (D4D) testing and legal aspects of passive deorbiting. Further details are available at http://REDSHIFT-H2020.EU/ .

Several mitigation-related presentations were made, with "Measuring the impact of the current level of adherence to Space Debris Mitigation guidelines" reviewing low Earth- and geosynchronous-orbit compliance and presenting a model for a proposed Space Debris Index. Remediation enabling analyses explored the long-term attitude dynamics subject to geomagnetic and other environmental influencers, relevant to resident space object attitude characterization and active debris removal. Remediation solutions, including laser orbit perturbation and engineering test articles, some currently on-orbit, were reviewed in detail. Among the latter were presentations on the RemoveDEBRIS mission, D-Sat, and planning for the removal and safe disposal of the large ENVISAT spacecraft.

Both the venue and the workshop organization, with ample time being available for questions and discussion between all participants, ensured an active workshop. Mr. Christophe Bonnal, CNES workshop organizer and long-time contributor to the orbital debris community, is to be recognized for his leadership in this very productive meeting. ♦

UPCOMING MEETINGS

11-14 September 2018: 19th Advanced Maui Optical and Space Surveillance Technologies Conference, Maui, Hawaii (USA)

The technical program of the 19th Advanced Maui Optical and Space Surveillance Technologies Conference (AMOS) will focus on subjects that are mission critical to Space Situational Awareness. This year's keynote speaker will be USAF Major General Whiting, Commander 14th Air Force, Air Force Space Command. The technical sessions include papers and posters on Orbital Debris, Space Situational Awareness, Adaptive Optics & Imaging, Astrodynamics, Non-resolved Object Characterization, and related topics. In addition, seven Technical Short Courses and the EMER-GEN program for students and young space professionals will be available to attendees. Detailed information about the conference is available at https://amostech.com.

1-5 October 2018: 69th International Astronautical Congress (IAC), Bremen, Germany

The IAC will convene in Bremen in 2018 with a theme of "IAC 2018 – involving everyone." The IAA will organize the 16th Symposium on Space Debris as session A6 during the congress. Nine dedicated sessions are planned to cover all aspects of orbital debris activities, including measurements, modeling, hypervelocity impact, mitigation, remediation, and policy/legal/economic challenges for environment management. An additional joint session with the section C1.7 Astrodynamics will be conducted. Additional information for the 2018 IAC is available at: https://www.iac2018.org/ .

14-19 April 2019: The 2019 Hypervelocity Impact Symposium, Destin, Florida (USA)

The Hypervelocity Impact Symposium (HVIS) is a biennial event organized by the Hypervelocity Impact Society that serves as the principal forum for the discussion, interchange, and presentation of the physics of high- and hypervelocity impact and related technical areas. The HVIS Symposia have a long-standing international reputation as a catalyst for stimulating research in this area through a wealth of oral and poster presentations, and commercial exhibits. The Symposium's proceedings are the major archival source of papers published in this field. Additional information for the 2019 Symposium is available at http://www.hvis.org/symposium.htm .

15-17 May 2019: 10th International Association for the Advancement of Space Safety (IAASS) Conference, El Segundo – Los Angeles, California (USA)

The 10th conference of the IAASS has as its theme "Making Safety Happen". Major debris-related topics include designing safety into space vehicles, space debris remediation, re-entry safety, nuclear safety for space missions, safety risk management and probabilistic risk assessment, and launch and in-orbit collision risk. In addition to the main sessions, four specialized sections will address Space Debris Reentries, Space Traffic Management, Safety Standards for Commercial Human Spaceflight, and Human Performance and Safety. Abstract submission deadline for the conference is 7 December 2018. Additional information for the 2019 IAASS is available at http://iaassconference2019.space-safety.org/ .

15-21 June 2019: 32nd International Symposium on Space Technology and Science, Fukui, Japan

The 32nd ISTS will be held in June 2019 in conjunction with the 9th Nano-Satellite Symposium (NSAT). This year's conference will be convened under the theme of "Fly Like a Phoenix to Space". Technical sessions include, but are not limited to, Space Environment and Debris; Space Situational Awareness; Reentry Safety; Hypervelocity Impact; Debris Risk Assessment and Management; Debris Mitigation and Removal; Space Law, Policy and International Cooperation; and Space Traffic Management. The abstract submission deadline is 31 October 2018. Additional information about the conference is available at http://www.ists.or.jp/index.html .

9-12 December 2019: The First International Orbital Debris Conference (IOC), Sugar Land, Texas (USA)

The first of this "once-every-4-years" conference will be initiated 9-12 December 2019 in Sugar Land (near Housotn), Texas, United States. The goal of the conference is to highlight orbital debris research activities in the United States and to foster collaborations with the international community. The 4-day conference will cover all aspects of micrometeoroid and orbital debris research, mission support, and other activities. Topics to be covered include radar, optical, in situ, and laboratory measurements; engineering, long-term environment, and reentry modeling; hypervelocity impacts and protection; mitigation, remediation, policy, and environment management. The first conference announcement will be available in late 2018. See additional information at https://www.hou.usra.edu/meetings/orbitaldebris2019/ .

SATELLITE BOX SCORE

(as of 04 July 2018, cataloged by the U.S. SPACE SURVEILLANCE NETWORK)

Country/ Organization	Payloads*	Rocket Bodies & Debris	Total
CHINA	312	3652	3964
CIS	1520	5069	6589
ESA	82	57	139
FRANCE	64	488	552
INDIA	89	117	206
JAPAN	173	111	284
USA	1663	4737	6400
OTHER	887	116	1003
TOTAL	4790	14347	19137

** active and defunct*

DAS 2.1 NOTICE

Attention DAS 2.1 Users: an updated solar flux table is available for use with DAS 2.1. Please go to the Orbital Debris Website at https://orbitaldebris.jsc.nasa.gov/mitigation/das.html to download the updated table and subscribe for email alerts of future updates.

Technical Editor
Phillip Anz-Meador, Ph.D.

Managing Editor
Debi Shoots

Correspondence concerning the ODQN can be sent to:

NASA Johnson Space Center
The Orbital Debris Program Office
X14-9E/Jacobs
Attn: Debi Shoots
Houston, TX 77058
debra.d.shoots@nasa.gov

National Aeronautics and Space Administration
Lyndon B. Johnson Space Center
2101 NASA Parkway
Houston, TX 77058

www.nasa.gov
https://orbitaldebris.jsc.nasa.gov/

INTERNATIONAL SPACE MISSIONS

01 April – 30 June 2018

International Designator	Payloads	Country/ Organization	Perigee Altitude (KM)	Apogee Altitude (KM)	Inclination (DEG)	Earth Orbital Rocket Bodies	Other Cataloged Debris
2018-032A	DRAGON CRS-14	USA	402	407	51.64	0	2
2018-033A	SUPERBIRD 8	JPN	35779	35795	0.02	1	1
2018-033B	HYLAS 4	UK	35779	35795	0.04		
2018-034A	YAOGAN-31 A	PRC	1079	1101	63.41	1	3
2018-034B	YAOGAN-31 B	PRC	1079	1101	63.41		
2018-034C	YAOGAN-31 C	PRC	1079	1101	63.41		
2018-034E	WEINA 1B	PRC	1078	1102	63.41		
2018-035A	IRNSS 1I	IND	35706	35866	28.67	1	0
2018-036A	USA 283	USA	NO ELEMENTS AVAILABLE			1	1
2018-036B	USA 284	USA	NO ELEMENTS AVAILABLE				
2018-036E	USA 285	USA	NO ELEMENTS AVAILABLE				
2018-036F	USA 286	USA	NO ELEMENTS AVAILABLE				
2018-036G	USA 287	USA	NO ELEMENTS AVAILABLE				
2018-037A	COSMOS 2526	CIS	35740	35758	0.05	1	2
2018-037B	BREEZE-M R/B	CIS	35766	41763	0.11		
2018-038A	TESS	USA	1056	355637	28.91	0	0
2018-039A	SENTINEL 3B	ESA	802	804	98.62	1	0
2018-040A	ZHUHAI-1 OHS-01	PRC	504	521	97.39	1	0
2018-040B	ZHUHAI-1 OVS-02	PRC	503	521	97.4		
2018-040C	ZHUHAI-1 OHS-02	PRC	504	521	97.4		
2018-040D	ZHUHAI-1 OHS-03	PRC	507	518	97.39		
2018-040E	ZHUHAI-1 OHS-04	PRC	509	516	97.4		
2018-041A	APSTAR 6C	PRC	35782	35793	0.04	1	0
2018-042A	INSIGHT	USA	HELIOCENTRIC			0	0
2018-042B	MARCO-A	USA	HELIOCENTRIC				
2018-042C	MARCO-B	USA	HELIOCENTRIC				
2018-043A	GAOFEN-5	PRC	698	703	98.13	1	0
1998-067NP	UBAKUSAT	TURK	399	399	51.64	0	0
1998-067NQ	1KUNS-PF	KEN	398	401	51.64		
1998-067NR	IRAZU	CRI	398	399	51.64		
2018-044A	BANGABANDHUSAT-1	BGD	35776	35797	0.02	1	0
2018-045A	QUEQIAO	PRC	EARTH-MOON L2			1	0
2018-045B	LONGJIANG 1	PRC	HELIOCENTRIC				
2018-045C	LONGJIANG 2	PRC	HELIOCENTRIC				
2018-046A	CYGNUS OA-9	USA	403	407	51.64	1	0
2018-047A	GRACE-FO 1	USA	481	509	88.99	0	1
2018-047B	GRACE-FO 2	USA	481	509	88.99		
2018-047C	IRIDIUM 161	USA	746	749	86.45		
2018-047D	IRIDIUM 152	USA	776	779	86.4		
2018-047E	IRIDIUM 147	USA	776	779	86.4		
2018-047F	IRIDIUM 110	USA	776	780	86.4		
2018-047G	IRIDIUM 162	USA	746	750	86.45		
2018-048A	GAOFEN 6	PRC	633	648	98.05	1	2
2018-048B	LUOJIA-1 01	PRC	632	649	98.05		
2018-049A	SES-12	SES	EN ROUTETO GEO			1	0
2018-050A	FENGYUN 2H	PRC	35775	35800	2.28	2	0
2018-051A	SOYUZ MS-09	CIS	403	407	51.64	1	0
2018-052A	IGS R-6	JPN	NO ELEMENTS AVAILABLE			1	1
2018-053A	COSMOS 2527 (GLONASS)	CIS	19122	19155	64.83	1	0
1998-067NT	REMOVEDEBRIS	UK	402	406	51.64	0	0
2018-054A	XJS A	PRC	478	486	35	1	1
2018-054B	XJS B	PRC	479	485	35		
2018-055A	DRAGON CRS-15	USA	403	407	51.64	0	2